Sustained Isobutene Production by *Synechocystis* Entrapped in Polyvinyl Alcohol Hydrogel Beads

Sindhujaa Vajravel, Sanjukta Aravind, Karin Stensjö*
Microbial Chemistry, Department of Chemistry-Ångström Laboratory, Uppsala University, SE-751 20, Uppsala, Sweden
* Corresponding author E-mail address: karin.stensjo@kemi.uu.se

Abstract

Cyanobacteria efficiently harness solar energy to convert CO_2 into valuable compounds, making them promising candidates for sustainable isobutene production -a key precursor for fuels and industrial chemicals. This study aimed to enhance isobutene photoproduction by using engineered *Synechocystis* strains, Syn-*Rn*KICD which produces isobutene from α-ketoisocaproate (KIC) via the heterologously expressed enzyme α-ketoisocaproate dioxygenase from *Rattus norvegicus* (*Rn*KICD), and Syn-F336V expressing a mutant variant of RnKICD with improved isobutene formation. We investigated the effect of environmental factors such as light intensity, inorganic carbon, and nitrogen levels on isobutene production. Our findings indicate that nitrogen limitation enhanced isobutene yields by reducing growth, likely due to decreased competition from branched-chain amino acid (BCAA) biosynthesis, increasing the availability of carbon precursors for isobutene synthesis. However, prolonged nitrogen limitation eventually constrained productivity, likely due to the imapairment of essential metabolic functions required for cell viability. To address this, we employed a cell entrapment strategy using polyvinyl alcohol with sodium alginate (PVA-SA) hydrogel beads crosslinked with borate and calcium ions to restrict growth while maintaining long-term isobutene production. By optimizing parameters such as crosslinking time, pH, and the hydrogel-to-cell mass ratio, we improved bead stability and prevented disintegration under bicarbonate-supplied inorganic carbon and nitrogen conditions. This approach improved the production of isobutene in Syn-*RnKICD* and Syn_F336V cells by approximately 60% and 80% respectively, compared to suspension-cultured cells. This study highlights critical environmental factors influencing isobutene production in *Synechocystis* and demonstrates that strategic growth restriction by cell entrapment can prolong isobutene productivity by optimizing metabolic efficiency.

Keywords

Photosynthesis, cyanobacteria, Isobutene, α-ketoisocaproate dioxygenase, Nitrogen limitation, Cell entrapment, Polyvinyl alcohol-sodium alginate hydrogel

Introduction

As global efforts to reduce reliance on fossil resources intensify, the push for renewable chemical production has become crucial for achieving sustainability and protecting the environment. Photosynthetic cyanobacteria are being recognized for their potential in sustainable chemical production, efficiently using sunlight and atmospheric CO_2 to synthesize valuable organic compounds. These microorganisms exhibit notable solar energy conversion efficiencies, reaching approximately 8–10% for solar-to-biomass conversion, surpassing the typical 4-6% efficiency observed in terrestrial plants (Melis, 2009; Zhu et al., 2008). Additionally, their rapid growth rates, high lipid content for biofuel production, and ability to thrive in diverse environments, including wastewater for potential bioremediation applications, make cyanobacteria efficient and environmentally friendly resources (Farrokh et al., 2019).

Cyanobacteria's genetic flexibility offers extensive bioengineering potantial to optimize photosynthetic pathways for efficient converting CO_2 into targeted organic molecules. Advances in synthetic biology and metabolic engineering have greatly expanded their capacity to produce a diverse array of chemicals. These include biofuels such as ethanol and butanol, industrial precursors like isoprene, isobutene, and ethylene, and other high-value compounds such as 2,3-butanediol, sucrose, lactic acid, isobutyraldehyde, and bisabolene (Angermayr et al., 2015; Carroll et al., 2018; Santos-Merino et al., 2019). Furthermore, photobiologically derived alkenes and dienes can be converted into sustainable kerosene-type fuel precursors through photochemical dimerization processes, showcasing the substantial potential of these microorganisms in producing renewable high-energy-density fuels (Rana et al., 2022). Additionally, the ability of these small, volatile hydrocarbon compounds to easily diffuse out of cyanobacterial cell membranes without damaging the cells enhances the energy efficiency of the product harvesting process (Lindberg et al., 2010; Ducat et al., 2011).

Isobutene (C_4H_8) is a highly versatile hydrocarbon pivotal in the chemical industry, primarily due to its reactive double bond that facilitates a variety of photochemical reactions. Its unique structural features allow it to be oligomerized and polymerized into a wide range of industrial products. Remarkably, isobutene can undergo visible light induced cationic photopolymerization, producing significant polymers such as plastics and rubbers (Hulnik et

al., 2023), underscoring its role in advanced materials science. Moreover, its oligomerization potential extends to creating jet-range fuels, showcasing its viability in sustainable fuel solutions (Hauge et al., 2005; Taylor et al., 2010; Peters and Taylor, 2013; Kostjuk 2015; Nicholas, 2017). These chemical reactions are particularly advantageous because they occur under mild conditions, which allow for precise control over reaction dynamics, offering significant benefits over traditional thermal processes. Despite these innovations, isobutene is still primarily sourced from fossil fuels, highlighting a significant opportunity and need for developing renewable production methods to meet the demands of the petrochemical industry sustainably.

Thus, the worldwide demand for environmentally sustainable isobutene production is growing rapidly, with projections estimating the market could reach USD 30.71 billion by 2024, and demand expected to surpass 16 million tons (Rebolledo-Leiva et al., 2022). The highest bioisobutene productivity reported so far is 0.45 mg/L/h by the yeast *Rhodotorula minut*a (Wilson et al., 2018), but to achieve economic viability, yields of approximately 2–4 g/L/h are necessary (van Leeuwen et al., 2012). Recent advancements focus on using metabolically engineered cyanobacteria while optimizing favorable environmental conditions to meet these economic and sustainability targets.

Our team has engineered the cyanobacterium *Synechocystis* sp. PCC 6803 to produce isobutene directly from CO_2 by heterologously expressing the *Rattus norvegicus* α-ketoisocaproate decarboxylase (*Rn*KICD), re-routing the central metabolism from pyruvate through the L-leucine biosynthesis pathway-derived metabolite α-ketoisocaproate (KIC) to isobutene, achieving a yield of 91 ng l^{-1} OD_{750}^{-1} h^{-1} (Mustila et al., 2021). The mammalian enzyme KICD, catalyzes the decarboxylation and oxygenation of KIC to form β-hydroxy-β-methyl butyrate (HMB) in the cytosol of liver cells as part of the L-leucine catabolic pathway (Sabourin & Bieber 1982). Thus, the *Rn*KICD acts on multiple substrates, catalyzing the conversion of 4-hydroxyphenylpyruvate (HPP) to homogentisate (HGA) and α-ketoisocaproate (KIC) to either HMB or isobutene. Building on these findings, our team recently refined *Rn*KICD's substrate preference for KIC to further boost isobutene production. Through protein engineering and targeted mutagenesis, a specific mutation, F336V, was identified, which shifts *Rn*KICD's substrate preference toward KIC, significantly enhancing isobutene production (Schumann et al., 2024). These advancements underscore the potential of engineered cyanobacteria for increased isobutene production. Further optimizations of

favorable culture conditions is essential to achieve production levels that meet commercial demands.

The efficiency of photosynthetic production in cyanobacteria is significantly influenced by various environmental conditions, including light intensity, pH, temperature, and the availability of macronutrients like inorganic carbon (Ci), nitrogen (Ni), phosphorus (Pi), and sulfur (Si) (Miller and Colman, 1980; Gordillo et al., 1998; Abm et al., 2019; Aboim et al., 2019; Rodrigues et al., 2023). However, traditional suspension cultures face yield limitations due to excessive biomass growth accumulation, which raises nutrient demand, increases oxidative stress, and causes self-shading effects, all of which can reduce the efficiency of light capture for photosynthesis (Chisti, 2007; Kim et al., 2011; Pedruzi et al., 2019).

A promising strategy to address these limitations is the entrapment of microalgal cells within natural biodegradable polymers. One widely used method involves crosslinking sodium alginate with $CaCl_2$ to create stable hydrogel beads. This process occurs through ionic bonds between Ca^{2+} ions and the carboxylate groups of guluronic and mannuronic acid residues in neighboring alginate chains, resulting in a robust three-dimensional network (Simpson et al., 2004). This cell-entrapping approach improved cyanobacterial viability and productivity, as evidenced by the enhanced production of ammonia, hydrogen, ethylene, β-phellandrene, and sucrose. These improvements were achieved by effective biomass growth mangement, even nutrient distribution, enhnced cellular communication, and reduced oxidative stress (Brouers and Hall, 1986; Kosourov et al., 2014; Vajravel et al., 2020; Valsami et al., 2021; Tóth et al., 2022). However, the use of Ca^{2+} alginate beads in cyanobacterial photoproduction systems can present challenges, particularly due to the potential formation of $CaCO_3$, which diminishes bead stability, especially in environments where $NaHCO_3$ is used as a crucial inorganic carbon source to produce small volatile hydrocarbons in air-tight vessels. (Rissanen et al., 2022).

Polyvinyl alcohol (PVA) hydrogels are widely used in biomedical applications due to their flexible crosslinking capabilities, biocompatibility, biodegradability, and cost (Zhong et al., 2024). PVA can be crosslinked using various methods, including sodium borate, boric acid, glutaraldehyde, formaldehyde, UV treatment and freeze-thawing (Wu & Wisecarver, 1992; Gohil et al., 2006; Bolto et al., 2009; Hua et al., 2010). Particularly, the simplicity and reversibility of the borate-PVA crosslinking mechanism make it an attractive option for drug delivery and tissue engineering. When borate ions ($B(OH)_4^-$) interact with PVA, they form

reversible covalent bonds with the hydroxyl groups of PVA, creating a stable and dynamic hydrogel structure (Cheng and Rodriguez, 1981; Wu & Wisecarver et al., 1992; Choe et al., 2024; Wu et al., 2024). The dynamic nature of this interaction supports repeated deformation and recovery, further improving the hydrogel's functionality across various applications.

In this study, we aimed to enhance isobutene production in *Synechocystis* strains, Syn-*Rn*KICD and Syn-F336V, by systematically exploring various environmental parameters, including light intensity, $NaHCO_3$ supplementation, nitrogen source availability, and cell entrapment. We employed borate-PVA hydrogel for cell entrapment. Our findings indicated that incorporating a stabilizing agent like sodium alginate (SA), adjusting the crosslinking duration, maintaining neutral pH conditions, and optimizing the cell biomass ratio to hydrogel significantly improved the stability and longevity of the hydrogel beads during HCO_3 supplementation as a crucial inorganic carbon source. By utilizing this optimized system, we extended the productive phase of isobutene production for a month, achieving maximum yields of ~ 94 mg/g DW in the entrapped Syn-F336V cells, which is about 65% higher than in the base strain, Syn-*Rn*KICD.

Materials and Methods

Strains and Growth Conditions

The two strains derived from *Synechocystis* sp. PCC 6803 employed in this study were previously constructed: Syn-*Rn*KICD, which produces a α-ketoisocaproate dioxygenase enzyme from *Rattus norvegicus* (*Rn*KICD) (Mustila et al., 2021), and Syn-F336V, in which a modified version of *Rn*KICD is produced (Schumann et al., 2024).

Synechocystis precultures were cultivated photoautotrophically in BG11 liquid medium in 6-well polystyrene plates, illuminated with continuous white light at a photosynthetic photon flux density (PPFD) of 30 µmol photons m^{-2} s^{-1}. For the standard cultivation of experimental cultures, 250 mL Erlenmeyer flasks (E-flasks) containing 80 mL of medium were buffered with 25 mM HEPES-NaOH (pH 7.4) and supplemented with 50 µg/mL kanamycin (Km). The cultures were supplied with 50 mM $NaHCO_3$ and maintained at 30°C with shaking at 100 rpm under illumination of 50 µmol photons m^{-2} s^{-1}. All strains were preserved at -80°C in 10% glycerol, and all precultures were initiated from cryopreserved cells.

Isobutene Production and Quantification

For isobutene production conditions, *Synechocystis* cells cultivated in E-flasks were harvested by centrifugation at 5000 rpm for 5 min at room temperature upon reaching an optical density (OD_{750}) of ~ 1. Following centrifugation, the cells were washed with fresh BG11 medium, adjusted to OD_{750} of 1, and supplemented with 50 mM $NaHCO_3$ (or as otherwise noted) and 50 µg/mL Km. A 10 mL aliquot of the cell suspension was transferred into 20 mL gas-tight vials, which were sealed with Teflon-coated septa to prevent hydrocarbon absorption.

The suspension culture vials were shaken at 120 rpm on a rotary shaker under an illumination of 50 µmol photons m^{-2} s^{-1} (unless stated otherwise). The headspace of the vials was sampled through the Teflon septum using a syringe every 24 h, with the septa replaced after each injection to minimize any loss of produced isobutene and to allow for CO_2 gas exchange from the air into the vials.

Isobutene detection and quantification were performed using an Agilent 7890A Gas Chromatography (GC) system coupled with a 5975 Mass Selective Detector (MSD), equipped with an HP-1ms Ultra I column. Samples were taken from 20 mL GC vials with Teflon-coated septa (VWR) and injected using a PAL-RSI85 autosampler with the PAL-HS2500 gas syringe tool. The GC-MS method for isobutene detection was adapted from Rossoni et al. (2015). Prior to injection, GC vials were incubated for 5 min at 40°C to equilibrate the isobutene concentration in the headspace. For detection, 100 µL of each sample were injected at an inlet liner temperature of 150°C with a 100:1 split ratio. The oven temperature was held at 40°C for 3 minutes before increasing by 30°C/min for 2 min. The retention time for isobutene was ~1.94 minutes with an authentic standard (99% v/v C_4H_8, AGA, Sweden). The MS detector operated in selected ion monitoring (SIM) mode to enhance sensitivity, specifically detecting isobutene signals at m/z 41 and 56. Signals within the chromatogram were analyzed for peak area through autointegration. The quantity of isobutene was determined from a calibration curve established using various dilution percentages of a commercial gas standard (99% v/v C_4H_8, AGA, Sweden). Isobutene productivity was normalized to the initial OD values for suspension cultures and initial cell dry weight was used for entrapped cells. For direct comparison of isobutene productivity between suspension and entrapped cells, the initial dry weight of cells was used.

The cumulative productivity of isobutene was calculated by summing the isobutene produced at 24-hour intervals. The data were averaged from three independent measurements taken from three replicates (±SD).

Induction of Nitrogen Starvation

Nitrogen starvation in *Synechocystis* cells was induced by omitting $NaNO_3$ from the BG-11 medium in the E-flask allowing for adaptation according to the previously specified experimental culture conditions. Different nitrogen adaptation periods were tested to assess the effects of both short-term (24 h) and long-term (72 h) nitrogen starvation on *Synechocystis* cells. After the adaptation periods, the cells were washed with nitrogen-free BG-11 medium by centrifuging at 5000 rpm for 5 min (2x). The washed cells were then resuspended in nitrogen-free medium and transferred into tightly sealed vials for isobutene production, following the conditions described previously in the isobutene production section.

Cell entrapment procedures

Syn-*Rn*KICD and Syn-F336V cells were cultivated under standard experimental conditions as outlined in the isobutene production section. Once the cells reached an optical density (OD_{750}) of 1, the cells were harvested by centrifugation at 5000 rpm for 5 min. Subsequently, the cyanobacterial cells were entrapped in hydrogel beads for immobilization, following the method described by Brouers and Hall (1986) with some modifications. We employed a PVA hydrogel crosslinked with boric acid (H_3BO_3) using a droplet-based dispersion technique via a 2 mL syringe. To enhance the properties of the hydrogel beads, 0.5% sodium alginate (SA) was incorporated into the 6% PVA hydrogel (PVA-SA), and crosslinking was achieved using 2% $CaCl_2$ and 4% H_3BO_3 solutions. The cell entrapment procedure involved varying formulations of wet cell biomass to PVA-SA hydrogel, specifically ranging from a ratio of 5:6:0.5 to 5:36:3 (cell:PVA:SA).

Hydrogel droplets were manually dispensed into the crosslinker solutions on Petri plates using a 2 mL syringe. After dispensation, the plates were sealed with Parafilm, and the crosslinking duration was optimized between 5 to 20 h. The beads were incubated at 30°C to complete the crosslinking process, illuminated with light at 30 μmol photons m^{-2} s^{-1}. Following crosslinking, the beads were thoroughly rinsed with sterile deionized water to remove excess crosslinkers and minimize ionic stress. The prepared entrapped cells in hydrogel beads were then transferred into 20 mL gas-tight vials containing BG11 medium with 50 mM NaHCO3 and subjected to the isobutene production conditions detailed earlier in the isobutene production section.

Measurement of cell density and pigment content

The growth of the cell cultures was assessed spectrophotometrically (Varian 50 Bio UV-Visible Spectrophotometer) by measuring the optical density at 750 nm (OD_{750}). The chlorophyll a (Chl a) content was quantified by measuring the absorbance at 665 nm following extraction with 90% methanol, in accordance with the method described by Lichtenthaler (1987). Additionally, the absorption spectra of the whole cell suspensions were recorded spectrophotometrically. Prior to measurement, all cultures were standardized to a uniform cell density of OD_{750} ~ 0.5.

Results and Discussion

Optimizing isobutene production in Syn-*Rn*KICD: The interplay of light intensity and inorganic carbon.

The main strain used in this study; Syn-*Rn*KICD, expresses the *Rn*KICD gene that encodes α-ketoisocaproate decarboxylase, an enzyme that has shown to convert α-ketoisocaproate (KIC) to isobutene *in vitro* and *in vivo* (Mustila et al., 2021). This reaction is key in redirecting metabolic carbon flux toward isobutene production in cyanobacteria (Mustila et al., 2021).

To study how varying light intensities affect isobutene production in we conducted experiments under three different photon flux densities: 35 (low), 85 (moderate), and 135 (high) µmol photons m^{-2} s^{-1}. To ensure adequate carbon availability for photosynthesis in the air-tight vessels all cultures were supplemented with 50 mM sodium bicarbonate ($NaHCO_3$) as inorganic carbon source. The optimal light intensity for maximizing isobutene yield was determined (Fig 1A)

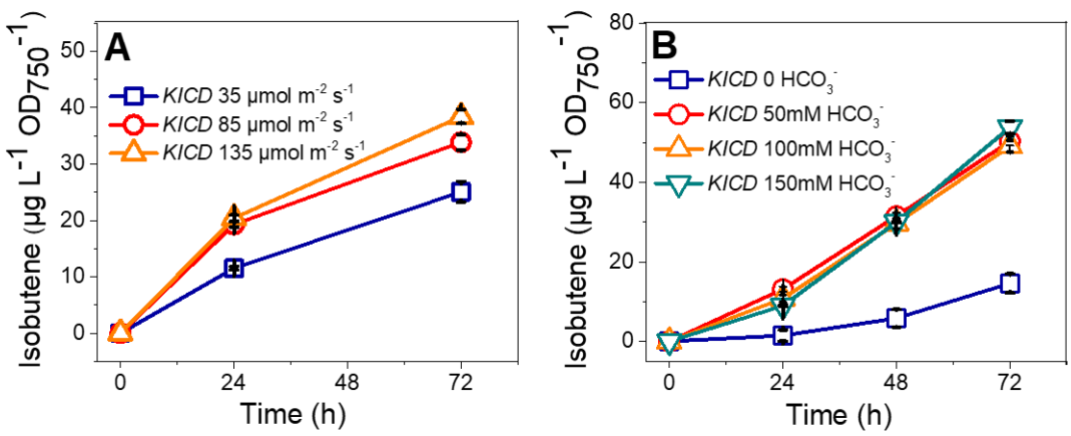

Figure 1: Influence of light intensity and inorganic carbon source on isobutene production in Syn-*Rn*KICD cells. A) Cumulative isobutene production measured in the headspace of closed culture vials. The cultures were exposed separately under three light intensities (35, 85, and 135 µmol photons m^{-2} s^{-1}). All cultures were uniformly supplemented with 50 mM $NaHCO_3$ as the inorganic carbon source. B) Isobutene productivity was assessed across a gradient of $NaHCO_3$ concentrations (0, 50, 100, and 150 mM) under high light intensity (135 µmol photons m^{-2} s^{-1}). The cumulative productivity of isobutene was calculated by summing the isobutene produced at 24-hour intervals and normalized to each cell culture's initial optical density measured at 750 nm (OD_{750}). The septa of the vials were changed after each injection to prevent any leakage of produced isobutene and to allow gas exchange providing CO_2 from the air. *KICD* refers to Syn-*Rn*KICD. Data shown are the average of three independent measurements from three replicates (±SD).

After 24 h, isobutene production in Syn-*Rn*KICD cells was ~11 µg L^{-1} OD_{750}^{-1} under low light intensity (Fig. 1A). Higher productivity levels of ~19 µg L^{-1} OD_{750}^{-1} and ~20 µg L^{-1} OD_{750}^{-1} were observed under moderate and high light, respectively. These findings indicate that while moderate and high light intensities lead to greater isobutene production than low light, the difference between moderate and high light intensities at 24 h was negligible. The increased isobutene production under moderate and high light was proportional to increased cell growth (OD_{750}) (Fig. S1A).

At 72 h, isobutene production reached ~25 µg L^{-1} OD_{750}^{-1} under low light intensity, ~33 µg L^{-1} OD_{750}^{-1} under moderate light, and ~38 µg L^{-1} OD_{750}^{-1} under high light (Fig. 1A). While high light intensity resulted in the highest isobutene production, it also caused cell bleaching and growth arrest by 72 hours (Fig. S1A). In contrast, cells exposed to low and moderate light showed no bleaching during this period. This suggests cell bleaching arises from an imbalance between light energy input and carbon assimilation. Prior studies indicate that cell bleaching can impair growth and productivity of *Synechocystis* (Van Alphen et al., 2018; Vajravel et al., 2021). Though adequate nutrient supply, including inorganic carbon, can mitigate light stress in cyanobacteria (Markou et al., 2014).

We hypothesized that excessive light energy relative to available inorganic carbon induces oxidative stress, leading to bleaching. To test this, cells were exposed to constant high light (135 µmol photons m^{-2} s^{-1}) and varying $NaHCO_3$ concentrations (0 to 150 mM). Cells

supplemented with higher concentrations of HCO_3^- (100 and 150 mM) did not exhibit bleaching at 72 h, while those with lower supplementation (50 mM) experienced bleaching and reduced growth (Fig. S1B). This suggests that insufficient levels of inorganic carbon under high light intensity disrupts energy homeostasis, causing oxidative stress and bleaching.

Isobutene production was observed across all conditions, but cells supplemented with HCO_3^- showed significantly higher productivity of isobutene and growth compared to the HCO_3^--deprived control cells. The maximum isobutene productivity (~53 μg L^{-1} OD_{750}^{-1}) was achieved with 150 mM HCO_3^-.That was nearly four-fold higher than in the control culture without added HCO_3^- (Fig. 1B). Although no significant difference in isobutene productivity was observed between 50 to 150 mM HCO_3^- supplementation (49–53 μg L^{-1} OD_{750}^{-1} at 72 h, Fig. 1B), bleaching occurred in cultures with low supplementation of HCO_3^- (50 mM) potentially impacting long-term isobutene production. Notably, control cells with lower isobutene production (14 μg L^{-1} OD_{750}^{-1} at 72 h, Fig. 1B) did not show bleaching but lacked substantial growth (Fig. S1B). This production likely originated from CO_2 in ambient air, during gas exchange, or stored carbon in the cells.

These results highlight the critical role of HCO_3^- in preventing bleaching under high light conditions in Syn-*Rn*KICD cells, as HCO_3^- serves as a key substrate for the Calvin cycle, the primary pathway of carbon fixation in cyanobacteria (Bennet, 1991; Miller et al., 1990; Badger and Price 2003). To balance the supply and demand side of photosynthetic metabolism, high light intensities increase the demand for carbon fixation. When HCO_3^- levels are limiting the isobutene production is competing with growth. Prior studies corroborate that excess light can trigger oxidative stress through ROS overproduction, decreasing photosynthetic efficiency and causing bleaching (Miller and Colman, 1980; Miller et al., 1990; Gordillo et al., 1998; Rodrigues et al., 2023). Our findings emphasize the need to balance light intensity and inorganic carbon availability to maintain *Synechocystis* cell viability and maximize isobutene production.

Impact of nitrogen limitation on the isobutene production in Syn-*Rn*KICD cells: Previous research by us implies that KIC serves as substrates for both isobutene and BCAA biosynthesis in *Synechocystis* (Mustila et al., 2021; Schumann et al., 2024). We reasoned that limiting N availability would decrease the metabolic flux toward BCAA synthesis, thus redirecting more carbon toward isobutene production. To test this hypothesis, we subjected Syn-*Rn*KICD cells

to N starvation and evaluated its effect on isobutene productivity (Fig. 2A) and pigment composition (Fig. 2B and 2C).

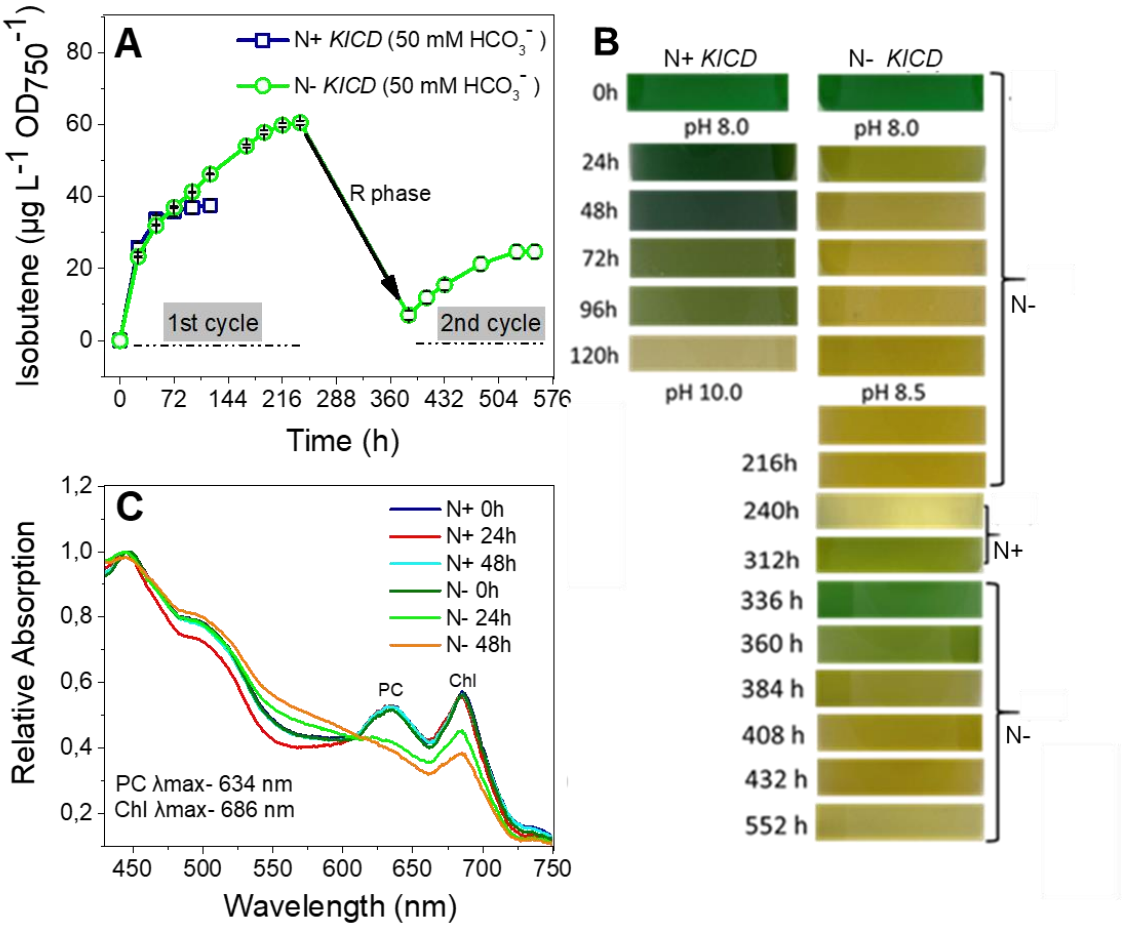

Figure 2: Impact of nitrogen limitation on isobutene production in Syn-*Rn*KICD. A) Isobutene productivity was periodically measured in cell cultures in BG11 medium supplemented with $NaNO_3$ (18 mM) (N+), and without (N-) The Syn-*Rn*KICD cells were cultivated with the appropriate medium for 24 h before being transferred to sealed vials for isobutene production. Isobutene was measured from the headspace of the vials every 24 h. B) Cell phenotypic changes were observed. C) Comparative whole-cell absorption spectra (ABS) were obtained to a similar optical density (OD_{750}) of the cells was set to ~0.5. ABS of cells showed phycobilin (λmax = 634 nm) and Chl a (λmax = 686 nm) peaks. The black arrow in Figure A indicates the resuscitation phase (R-Phase), where the reintroduction of $NaNO_3$ to the N- cells facilitated a recovery process, and a subsequent cycle of N starvation was instituted. All the cultures were maintained under an optimal light intensity of 50 µmol m^{-2} s^{-1} with 50 mM $NaHCO_3$. Isobutene productivity was normalized to the initial OD_{750} values of cells, and initial OD values were set

to similar in all the experimental setups. These results are the average of 3 independent measurements from 3 replicates (±SD). *KICD* refers to Syn-*Rn*KICD.

The nitrogen limitation experiments provide valuable insights into how nitrogen (N) manipulation impacts the partitioning of carbon fluxes between competing biosynthetic pathways in Syn-*RnKICD*. The cells were incubated under 50 µmol photons m^{-2} s^{-1} light intensity with addition of 50 mM NaHCO to prevent high light-induced damage. N starvation was induced by omitting $NaNO_3$ from the BG11 medium, the sole N source for the non-nitrogen-fixing *Synechocystis*.

Results revealed that isobutene production occurred regardless of N supplementation (Fig. 2A). However, N starved cells (N-) exhibited chlorosis after 24 h (Fig. 2B), indicating reduced photosynthetic pigments, particularly phycobilins (PB) and chlorophyll (Chl) (Fig. 2C). A sharp decrease in PB-to-Chl ratio, a known marker of N deprivation in *Synechocystis*, was also observed (Allen and Smith, 1969; Allen et al.,1990). Up to 72 h, there was no significant difference in isobutene production between N supplemented (N+) and N- cells (Fig. 2A). However, beyond 96 h, N- cells outperformed N+ cells producing approximately 46 µg L^{-1} OD_{750}^{-1} of isobutene at 120 h, which was 1.2 times the amount produced by N+ cells (37 µg L^{-1} OD_{750}^{-1}). At this point, N+ cells showed stagnation in isobutene production (Fig. 2A), along with severe cell bleaching and significant pigment loss (Fig. 2B). Remarkably, N- cells continued to produce isobutene up to 216 h, reaching ~60 µg L^{-1} OD_{750}^{-1} (Fig. 2A).

Although both N+ and N- cells had similar isobutene production rates up to 48 h (Fig. S2A), N- cells outperformed N+ cells from 72 h onward (Fig. S2A). Under these optimized conditions, the rate of in cell isobutene production was enhanced ten-fold as compared to the levels reported in our prior work (Mustila et al., 2021).

Initial growth, as measured by OD_{750}, and Chl content, was two- to four-fold higher in N+ cells than in N- cells up to 72 hours (Fig. S2B and S2C). At 96 h, N+ cells showed a rapid decrease in photosynthetic pigments (Fig. S2D). By 120 h, no pigment peaks were detected, likely leading to cell bleaching and reduced isobutene production. In contrast, N- cells maintained pigments levels for longer (Fig. 2B), but with a gradual decline between 48 and 120 h (Fig. S2E), and continued to produce isobutene until 216 h (Fig. 2A).

To explore recovery in N- cells $NaNO_3$ was reintroduced at 252 h. During resuscitation (R-phase), N- cells regenerated photosynthetic pigments (Fig. 2B) along with increased OD, Chl content and PB levels (Fig. S2B, C, and F) (Forchhammer & Schwarz, 2019). After reintroducing N depletion at 120 h, isobutene production resumed, though at lower levels than in first cycle (Fig. 2A). By the end of the second cycle, N- cells produced ~84 μg L^{-1} OD_{750}^{-1} of isobutene (totalling 552 h), demonstrating prolonged viability and enhances isobutene production compared to N+ cells under optimized conditions with 50 mM $NaHCO_3$, supplementation.

These results suggest that N limitation prolong cell viability and ability to produce isobutene under high-light conditions by preventing pigment loss and mitigating bleaching. Further, the recovery after NO_3^- reintroduction highlights the potential for cyclic N manipulation to optimize long-term isobutene productivity.

A key question is why well-grown N+ cells bleached and stopped producing isobutene despite being under standard light conditions (50 μmol photons m^{-2} s^{-1}) and with 50 mM HCO_3^- supplementation. It is important to note that bleaching occurred later under these conditions (120 h, Fig. 2B) as compared to under high-light (135 μmol photons m^{-2} s^{-1}), where bleaching was observed already at 72 h (Fig. S1B). The bleaching in N+ cells may be attributed to carbon limitation probably caused by the competition between overgrowth and isobutene production in air-tight vials with HCO_3^- supplementation. In contrast, N+ cells grown in E-flasks did not bleach even after two weeks (data not shown), likely due to the sufficient supply of inorganic carbon from ambient air through the cotton-sealed flasks.

Surprisingly, N- cells, maintained isobutene production over 552 h (Fig. 2A). Previous studies have shown that N starvation induces chlorosis in cyanobacteria, starting with the degradation of nitrogen-rich phycobiliproteins, to supply essential nutrients for cell survival (Allen & Smith, 1969; Spat et al., 2018). Chlorosis leads to a dormant state in which cell growth is arrested, and low-level photosynthesis is maintained as a long-term survival mechanism (Forchhammer & Schwarz, 2019; Forchhammer & Selim, 2020). Despite this, carbon fixation can still occur in N- cells, albeit at lower levels (Allen et al., 1990). In line with these findings, our results showed a significant growth difference between N+ and N- cells (Fig. S2B and S2C). N+ cells showed a 4.7-fold increase in OD, while N- cells had a 2-fold increase after 48 h (Fig. S2B and S2C). N- cells may still fix CO_2 using HCO_3^-, and direct the carbon toward

isobutene production rather than cell growth. These results suggest that the restricted growth in N- cells may prolong survival and enable sustained isobutene production over time.

Impact of prolonged nitrogen starvation on isobutene production in Syn-*Rn*KICD cells

To investigate whether prolonged growth restriction would enhance isobutene productivity in a shorter time, we extended the duration of N starvation in Syn-*Rn*KICD cultures. Unlike previous experiments where experimental cultures were subjected to 24 h of N starvation, resulting in two-fold higher growth than their initial period (Fig. S2B), the cells in this experiment underwent 72 h of N starvation. After this period, the cells were refreshed with the appropriate BG11 medium and transferred into tightly sealed vials for isobutene production. The results showed that prolonged N starvation increased isobutene production at 48 h (29 μg L^{-1} OD_{750}^{-1}), compared to in N supplemented cells (24 μg L^{-1} OD_{750}^{-1}) (Fig. 3A). Moreover, the N- cells showed consistent in the rate of isobutene production over 120 h (Fig. S2A). In these cells, OD_{750} only slightly increased 1.5-fold as compared the initial OD (Fig. S3B and C). At 120 h, N- cells still displayed pigment peaks in the absorption spectra, whereas no pigments were detected in the N+ cells (Fig. S3D and F). Correspondingly, N+ cells showed a decline in isobutene production by 120 h, whereas N- cells continued producing isobutene until 168 h, reaching a productivity of 57 μg L^{-1} OD_{750}^{-1}, nearly double that of N+ cells (30 μg L^{-1} OD_{750}^{-1}) (Fig. 3A). In 72 h, N starved cells, maximum isobutene productivity was observed at 168 h (Fig. 3A), whereas cells with 24 h of N starvation adaptation in the precultures required 216 h to reach the same level of production (Fig. 2A). These results confirm that substantial growth limitation in this prolonged N starved cells can enhance isobutene production within a shorter timeframe, possibly by redirecting carbon flux toward isobutene production.

To assess if severe bleaching in N+ cells was caused by competition for limited carbon between growth and isobutene production, we analysed cells with doubled nitrogen content (2xN) assuming that this would enhance initial growth. We incubated cultures with 2xN (36 mM $NaNO_3$) and 50 mM HCO_3^-. Results showed faster cell growth in 2xN cells by 48 h (Fig. 3B), accompanied by slightly higher OD and Chl levels at 24 and 48 h, respectively, compared to N+ cells (Fig. S3B and C). This accelerated growth-mediated carbon limitation, seen as bleaching already at 72 hours as compared to at 120h for the N+ cells (Fig. 3B), likely contributed to the marginally lower isobutene production in 2xN cells (28 μg L^{-1} OD_{750}^{-1}) compared to N+ cells (30 μg L^{-1} OD_{750}^{-1}) (Fig. 3A).

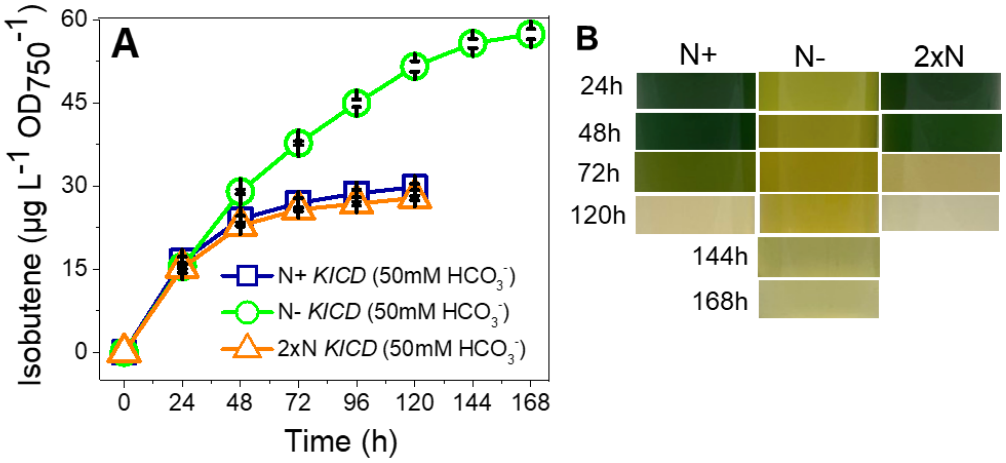

Figure 3: Impact of prolonged Nitrogen limitation on isobutene productivity in *Synechocystis KICD* cells. A) The cumulative isobutene productivity was evaluated in *KICD* cells under three distinct N conditions: N+, N-, and double N (2xN). The cells were incubated in appropriate preculture conditions for at least 72 h. Subsequently, the cells were transferred into tightly sealed vials for isobutene production. B) Phenotypic changes of the cells were documented. The cultures were illuminated with 50 µmol photons m^{-2} s^{-1} and supplied with 50 mM $NaHCO_3$. The isobutene productivity was normalized on the initial OD_{750} values of the cells. These results are the average of 3 independent measurements from 3 replicates (±SD). *KICD* refers to Syn-*Rn*KICD

The degradation of pigments were faster in 2xN cells, with no detectable pigments at 96 h (Fig. S3E), whereas N+ cells still showed detectable Chl peaks at that time (Fig. S3D). These findings confirm that the initial increased growth in 2xN cells resulted in a faster bleaching than in N+ cells, suggesting that competition between cell growth and isobutene production can lead to carbon limitation in the tightly sealed vials which, over time, negatively affects isobutene production under N+ conditions. Under N limitation, growth is reduced, likely at least partly due to decreased BCAA biosynthesis. The limited growth leads to metabolic redirection of carbon toward isobutene production. As a result, isobutene formation becomes less dependent on growth, with carbon flux shifting away from BCAA biosynthesis toward isobutene production.

Influence of carbon limitation on isobutene production in Syn-*Rn*KICD cells

To explore whether restricting the growth of Syn-*Rn*KICD cells under N+ conditions affects isobutene production, an experiment was conducted in which no $NaHCO_3$ was added to the

cultures (N+, N-, and 2xN). The results showed no noticeable difference in isobutene productivity up to 144 h in the C starved cells across the three culture conditions (Fig. 4A). N- cells still exhibited chlorosis-induced pigment loss, while N+ cells showed limited growth in the absence of HCO_3^- (Fig. 4B). Negligible growth was observed in both N+ and N- cells across all cultures (Fig. S4A), whereas 2xN cells showed a slight decline in growth. A noticeable reduction in OD_{750} levels was observed at 72 h across all cultures lacking HCO_3^- supplementation (Fig. S4A).

A significant decrease in the absorption peaks of photosynthetic pigments was observed in N+ cells after 96 h (Fig. S4B andC). In contrast, N- cells did not show substantial changes in pigment peaks after 24 h (Fig. S4D). A notable decrease in the PB ratio occurred during the initial transition in N- cells. Interestingly, all cells continued to produce isobutene at a low rate for an extended period (up to 144 h). This study demonstrated that in the absence of HCO_3^- no significant difference in isobutene productivity was observed between N+ and N- cells, with production levels ranging from 18 to 19 μg L^{-1} OD_{750}^{-1} (Fig. 4A). However, it is important to note that without HCO_3^-, overall isobutene productivity dropped significantly to 10 and 9 μg L^{-1} OD_{750}^{-1} at 72 h (Fig. 4A), much lower than the 35 and 38 μg L^{-1} OD_{750}^{-1} achieved with HCO_3^- supplementation at the same time point (Fig. 2A) in N+ and N- cells, respectively. These findings highlight that the differences in isobutene production between N+ and N- are only observed in the presence of HCO_3^-.

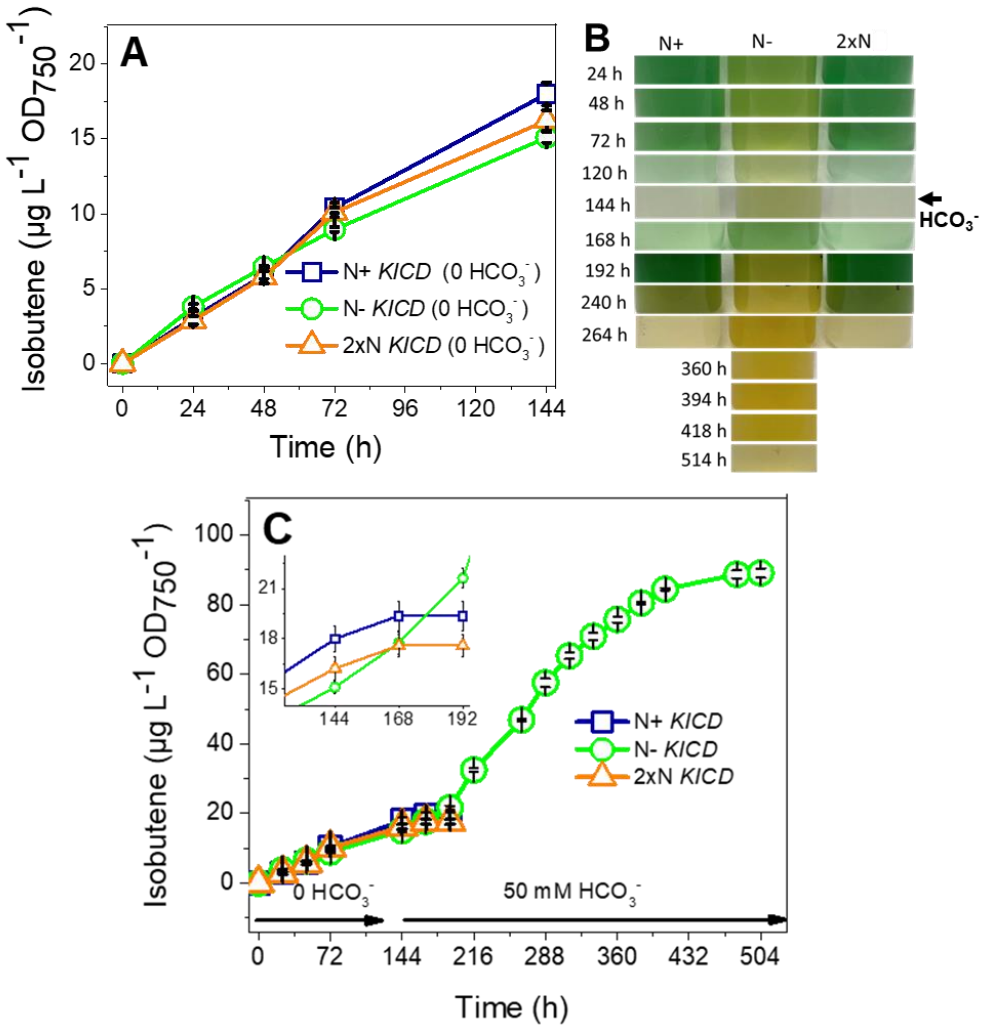

Figure 4: Impact of N and C depletion on isobutene production in Syn-*Rn*KICD cells. A) The cumulative isobutene productivity was evaluated in Syn-*Rn*KICD cells under three distinct conditions: N+, N-, and 2xN without HCO_3^-. B) The phenotypic changes in the cells were documented. C) cumulative isobutene productivity was evaluated in Syn-*Rn*KICD cells under three distinct conditions: N+, N-, and 2xN with 50 mM HCO_3^-. The experimental cultures in the E-flask were adapted in the appropriate medium for 24 h and then transferred into the closed vials for the production conditions. This experiment was carried out under illumination of 50 µmol photons m^{-2} s^{-1}. The isobutene productivity was normalized based on the initial OD_{750} values of the cells. These results are the average of 3 independent measurements from 3 replicates (±SD). *KICD* refers to Syn-*Rn*KICD

To investigate if supplementation of HCO_3^- can initiate cell growth and isobutene production in carbon-deprived cells, HCO_3^- was added to all cultures at 144 h (Fig. 4B). All cultures exhibited growth, as indicated by phenotypic changes observed at 192 h (Fig. 4B).

However, increased isobutene production after addition of HCO_3^- was only observed in N- cells. In contrast, no significant increase was seen in N+ cells, which, on the other hand, show a substantial increase in cell growth (Fig. 4B), probably leading to a depletion of carbon source and, thus, the ability to produce isobutene diminished. N- cells continued producing isobutene for 480 h, reaching approximately 89 µg L^{-1} OD_{750}^{-1}. These results emphasised that CO_2 fixation using inorganic carbon source HCO_3^- is rather directed toward isobutene production than to growth in N- cells. Furthermore, the observed difference in isobutene production between N+ and N- cells seems to be primarily due differences in growth, which were influenced by the addition of HCO_3^-.

Assessment of isobutene production in Syn-F336V cells under nitrogen starvation

In our previous work we show that by engineering the enzyme *Rn*KICD towards enhanced substrate specificity a four-fold increase in isobutene production from Syn-F336V was achieved (Schumann et al., 2024). Here we examine the effects of N starvation on isobutene production in the Syn-F336V cells to determine if the earlier observed results were specific to the unmodified *Rn*KICD enzyme or represented a broader metabolic shift. We expect Syn-F336V cells to reach higher production level of isobutene than Syn-*Rn*KICD also under nitrogen limitation. This expectation stems from two key factors: the reduced BCAA synthesis under N limitation, which redirects more carbon precursors toward isobutene production, and the F336V's improved ability use KIC over HPP as substrate. This approach can help to clarify how cultivation and enzyme optimization can synergistically increase isobutene yields.

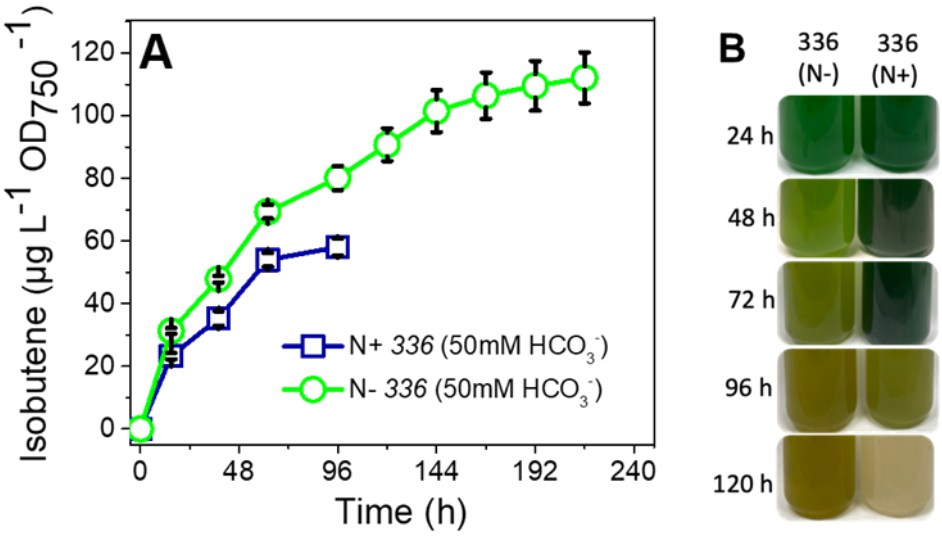

Figure 5: Impact of nitrogen limitation on isobutene production in Syn-F336V cells. A) The cumulative productivity of isobutene was periodically measured in the cells incubated with and without $NaNO_3$ in BG11 medium. B) The changes in the cells' phenotypic morphology were monitored every 24 h. The cultures were incubated under 50 μmol photons m^{-2} s^{-1} light intensity with supplementation of 50 mM $NaHCO_3$ in tightly sealed vials. The isobutene productivity was normalized to the initial OD_{750} values. The initial OD_{750} value was set similarly in all the cultures. In the figure, *336* refers to Syn-F336V and *KICD* refers to Syn-*Rn*KICD. These results are the average of 3 independent measurements from 3 replicates (±SD).

Our results showed that under normal nitrogen conditions (N+), the Syn-F336V cells exhibited a notable increase in isobutene production, reaching 60 μg L^{-1} OD_{750}^{-1} at 96 h (Fig. 5A). This represents a 1.6-fold increase compared to the isobutene production of the original Syn-*Rn*KICD cells (37 μg L^{-1} OD_{750}^{-1}) under identical conditions (Fig. 2A). This confirmed that the engineered Syn-F336V cells are significantly more efficient at producing isobutene than the Syn-*Rn*KICD cells. When subjected to N starvation (N-), the Syn-F336V cells showed even higher isobutene production, reaching ~80 μg L^{-1} OD_{750}^{-1} at 96 h, surpassing the productivity of the Syn-F336V cells (Fig. 5A). N+ Syn-F336V cells, like N+ Syn-*Rn*KICD cells, displayed increased growth up to 72 h, followed by cell bleaching at 96 h (Fig. 5B), with a decline in isobutene production. In contrast, under N- conditions, Syn-F336V cells exhibited chlorosis, a typical symptom of N starvation. Despite this, the isobutene production continued to increase, similar to N- Syn-*Rn*KICD cells, reaching ~120 μg L^{-1} OD_{750}^{-1} at 216 h (Fig. 5A). The peak in isobutene productivity of the Syn-F336V cells was two-fold higher than in the N starved Syn-*Rn*KICD cells over the same period (Fig. 2A). These results suggest that the Syn-F336V cells benefits from both reduced BCAA biosynthesis under N limitation and increased substrate specificity of the KICD enzyme towards KIC, leading to enhanced isobutene production. The observation that both Syn-*Rn*KICD and Syn-F336V cells showed increased isobutene production under N limitation suggests that this response is specific to the synthetic isobutene production pathway in *Synechocystis* cells, in which leucin and isobutene production compete for the same substrate; KIC.

Taken together the results suggest that in N+ cells supplied with HCO_3^- a competition for carbon may occur between growth and isobutene production. This competition will eventually lead to carbon limitation, inducing metabolic stress and cell damage in closed culture vials, as shown in Figures 2 to 5. Conversely, N starved-induced growth arrest in N-

cells could direct the supplied inorganic carbon primarily toward isobutene production for an extended period, as evidenced in Figures 2 to 5. Although N starved cells exhibited higher isobutene production compared to N+ cells under HCO_3^--supplemented conditions (Figs. 2-5), it is essential to acknowledge that these cells experience significant nutrient stress, leading to substantial losses of major photosynthetic pigments (Figs. S2 and S3). Previous studies have shown that while N starved cells can sustain low levels of photosynthesis (Sauer et al., 2001) and CO_2 fixation (Allen et al.,1990), this compromised photosynthetic capacity may ultimately limit long-term cell survival. Thus, utilizing N starved cells may not be ideal for maximizing isobutene production. Based on these findings, we propose that long-term improvements in isobutene production can be achieved by implementing strategies restricting cell growth while providing optimal $NaNO_3$ and HCO_3^- concentrations to *Synechocystis* cells. These cells should be cultured in media containing all essential macronutrients, including nitrogen, to maintain robust metabolic function.

Entrapment of Syn-*Rn*KICD cells in PVA hydrogel beads In this section, we aim to prolong cell viability and enhance isobutene production in Syn-*Rn*KICD and Syn-F336V cells by limiting cell growth through the controlled availability of inorganic carbon and nitrogen sources. We exploited a cell entrapment approach using PVA hydrogel crosslinked with borate ions ($B(OH)_4^-$). The rationale behind this approach is that physically entrapping cyanobacterial cells restrict their growth, redirecting energy and carbon utilization toward product synthesis instead of biomass accumulation, as supported by previous studies (Kosourov et al., 2014; Kosourov et al., 2018; Vajravel et al., 2020). During the droplet-based bead formation process, using a 5:6 ratio of cell wet weight to PVA hydrogel, we encountered a challenge: the PVA hydrogel tended to adhere, preventing the formation of distinct beads in the presence of the crosslinking agent boric acid (H_3BO_3). This issue may have resulted from insufficient electrostatic repulsion or steric stabilization among the PVA hydrogel particles, leading to clumping (Wu & Wisecarver et al 1992). To address this, we incorporated a small amount of sodium alginate (SA, 0.5%) into the PVA hydrogel mix. SA can facilitate bead formation due to its ability to form crosslinked structures via ionic interactions, enhancing stabilization.

Following this modification, distinct hydrogel beads were promptly generated in this study, when the cell-PVA-SA mixture, at a 5:6:0.5 ratio, was introduced into a solution of crosslinking agents, H_3BO_3 (4%) and $CaCl_2$ (2%). We first evaluated the effects of entrapping Syn-*Rn*KICD cells in PVA hydrogel beads with HCO_3^- supplementation. After crosslinking

for 5 h at 30 °C, the beads initially appeared stable. However, upon the addition of HCO_3^-, bead-disintegration was observed at 24 h, resulting in a free-cell suspension (Fig. 6A). The shorter crosslinking duration may have contributed to the early breakdown of the beads. The kinetic energy of molecules is temperature-dependent, and at 30 °C, the crosslinking reaction between PVA and borate ions may have proceeded more slowly. This reduced kinetic energy could have delayed the interactions necessary for effective crosslink formation. Despite this limitation, maintaining a temperature of 30 °C is essential, as it is optimal for *Synechocystis* growth. Therefore, optimizing the crosslinking conditions within this temperature constraint is critical to ensuring hydrogel stability and optimal cellular function. In our following approach, we extended the crosslinking duration from 5 h to 20 h without changing the crosslinking temperature, aiming to strengthen the interactions between the hydrogel and crosslinking agents, thereby creating a more stable hydrogel structure (Fig. 6B).

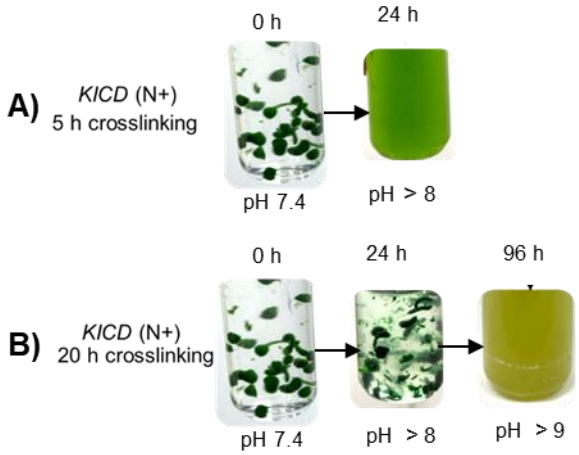

Figure 6: Influence of crosslinking duration on the stability of *Synechocystis* hydrogel beads. A) After 5 h of crosslinking duration, stable beads were observed up to 24 h following the addition of $NaHCO_3$ (50 mM). B) With a crosslinking duration of 20 h, bead stability was maintained for up to 96 h after adding HCO_3. A 5:6:0.5 ratio of cell wet mass: PVA: SA) was employed for droplet-based cell entrapment using H_3BO_3 (4%) and $CaCl_2$ (2%) crosslinking agents. After crosslinking, the entrapped cells were refreshed with BG11 medium, transferred into tightly sealed vials, illuminated with 50 µmol photons m^{-2} s^{-1}, and supplemented with 50 mM $NaHCO_3$. *KICD* refers to Syn-*Rn*KICD

Although the extended crosslinking time (20 h) showed an increased stability initially, the beads began to disintegrate after 96 h $NaHCO_3$ incubation (Fig. 6B). These results suggest that while longer crosslinking can postpone bead breakdown in the presence of $NaHCO_3$, it cannot completely prevent it. We also observed a significant increase in pH, from ~ 7.4 to 9, in the

entrapped cell cultures. Despite initially supplementing the entrapped cells with a buffered medium, the addition of 50 mM $NaHCO_3$ likely contributed to the pH rise. An increase in alkaline pH can destabilize PVA-SA beads crosslinked by $B(OH)_4^-$ and Ca^{2+} ions by altering the ionization states, weakening crosslink density, and potentially causing excessive swelling or hydrolysis. This destabilization may have led to bead disintegration and the release of free cells into the medium.

Effect of pH on the stability of entrapped Syn-*Rn*KICD hydrogel beads and isobutene production

Our previous experimental results indicated that the stability of PVA-SA hydrogel beads may be compromised under alkaline conditions (Fig. 6). Although *Synechocystis* typically thrives in a pH range of 7.0 to 9.0, maintaining a neutral pH (~7) could be essential for preventing bead disintegration and ensuring cell viability. By adjusting the medium's pH to neutral every 24 h, we observed that the hydrogel beads remained stable without disintegration, even after 96 h of incubation with HCO_3^- (Fig. 7A). These results underscore the critical importance of maintaining a neutral pH for the stability of entrapped cells in the PVA-SA hydrogel beads. Next, we investigated the isobutene-producing capacity of entrapped Syn-*Rn*KICD cells within these hydrogel beads. After 120 h from bead formation, the entrapped Syn-*Rn*KICD cells were transferred into tightly sealed vials and exposed to constant light at 50 μmol m^{-2} s^{-1}. We monitored isobutene productivity in the headspace of the vials at 24 h intervals. Remarkably, isobutene production was observed at 144 h after bead formation or 24 h following their light adaptation period, as shown in Fig. 7B. The isobutene productivity persisted over 336 h post-bead formation, achieving a productivity of ~40 mg/g DW after 216 h post-adaptation under continuous illumination.

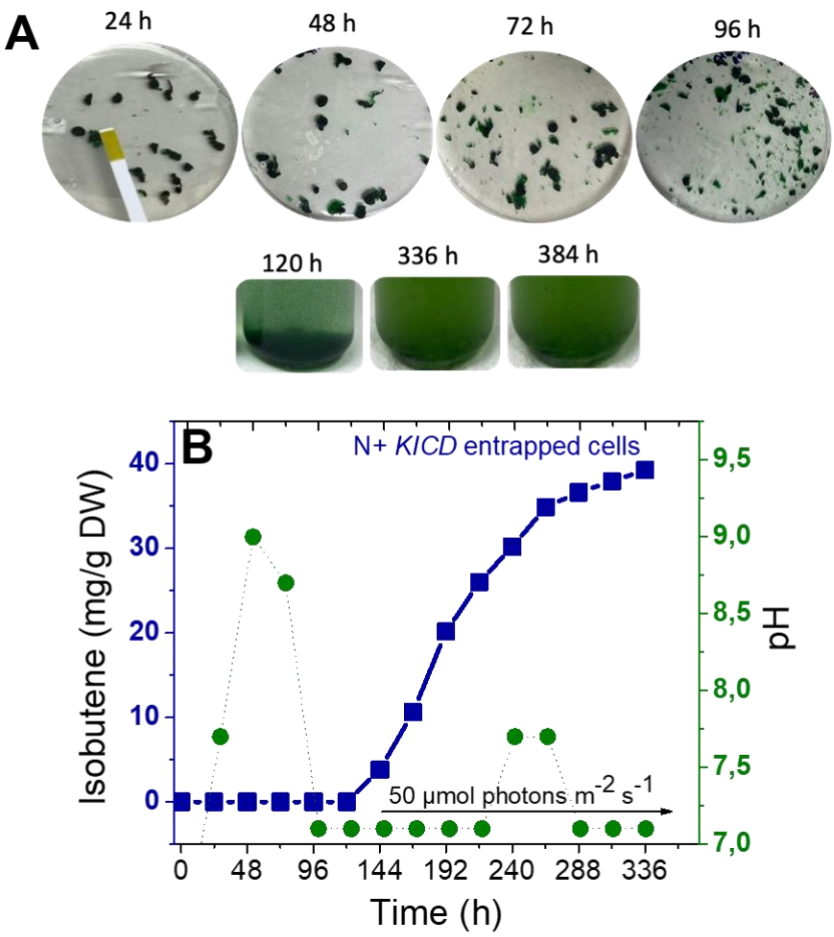

Figure 7: Influence of pH on the stability of Syn-*Rn*KICD cells entrapped in PVA-SA hydrogel beads. A) The phenotypic changes of the hydrogel beads were observed in the presence of 50 mM HCO_3^-, with the pH level adjusted at ~7 with 5N HCl throughout the experiment. B) The cumulative isobutene production from the entrapped cells was monitored. The cell entrapment was performed using the following formulation: 5:6:0.5 (wet cell:PVA: SA). These hydrogel beads containing cells were crosslinked with H_3BO_3 (4%) and $CaCl_2$ (2%) for 20 h. After 20 h of crosslinking, the entrapped cells were refreshed with BG11 medium, illuminated with 50 µmol photons m^{-2} s^{-1}. The productivity of isobutene was normalized on the initial dry weight of the cells. *KICD* refers to Syn-*Rn*KICD.

This observation is particularly notable when compared to the rapid bleaching and cessation of isobutene production observed within 120 h in a comparable N+ Syn-*Rn*KICD liquid culture (Fig. 2). In contrast, entrapped cells within the PVA-SA hydrogel did not show any cell bleaching, even after 216 h of incubation in tightly sealed vials, as evidenced by their phenotypic morphology. However, partial bead disintegration was observed after 336 h of bead formation (Fig. 7A). These non-bleaching cells likely contributed to the extended period of

isobutene production for 336 h (Fig. 7B). These results demonstrate that maintaining a neutral pH in the entrapped cell cultures can enhance the structural integrity of the PVA-SA hydrogel beads, which, in turn, could prevent cell bleaching and promotes long-term isobutene production. However, despite maintaining a neutral pH, the beads were unstable over an extended period. Free-floating cell suspensions were observed, and distinct beads were no longer visually detectable after 336 h (Fig. 7A). This disintegration of the beads could be due to excessive cell growth over time under N+ and with addition of HCO_3^-. This points to the eventual limitations of hydrogel bead stability and underscores the need to optimize the cell-to-hydrogel ratio to limit cell growth strictly and thus to improve bead stability further.

Impact of a two-fold increase in hydrogel-to-cell ratio on the stability of entrapped cells: In our continued efforts to improve the stability of the entrapped cells' beads and enhance isobutene productivity, we focused on the effect of increasing the hydrogel-to-biomass ratio. Considering that denser hydrogel beads may further restrict cell expansion and proliferation, we adjusted the cell wet biomass to PVA-SA ratio from 5:6:0.5 to 5:12:1 while maintaining a neutral pH throughout the experiment. This experiment was designed to investigate how an increase in the hydrogel-to-biomass ratio, combined with neutral pH adjustments, influences bead stability and isobutene production in the presence of HCO_3^-. Additionally, we examined the entrapped cells under N+ and N- conditions. This was motivated by our earlier observations in this study that N+ conditions promote more significant cell growth, whereas N- conditions limit cell growth. This comparison can help us better understand the different growth dynamics of entrapped cells within hydrogel beads, especially in an HCO_3^- environment. Before bead formation, Syn-*Rn*KICD cells were acclimated to the appropriate growth conditions (N+ and N-) for 24 h in liquid culture. The crosslinking phase resulted in distinct and stable bead formation, as evidenced by their phenotypic morphology (Fig. S5). We then monitored isobutene production in the entrapped cells at 24-hour intervals in tightly sealed vials.

The results showed no significant difference in isobutene productivity between N+ and N- entrapped cells up to 72 h (Fig. 8A). However, at 96 h, N- cells exhibited higher isobutene production, reaching ~28 mg/g DW at 144 h, while N+ cells produced ~19 mg/g DW. Although the beads remained stable up to 144 h under both N+ and N- conditions, partial disintegration was observed in N+ beads starting at 192 h, as shown by their phenotypic morphology (Fig. 8B). However, isobutene productivity continued to increase under both conditions (Fig. 8A). At 216 h, 25 mM HCO_3^- was added to study if the isobutene production could be further

increased. This addition slightly improved isobutene production in both N+ and N- cells from 264 h onwards.

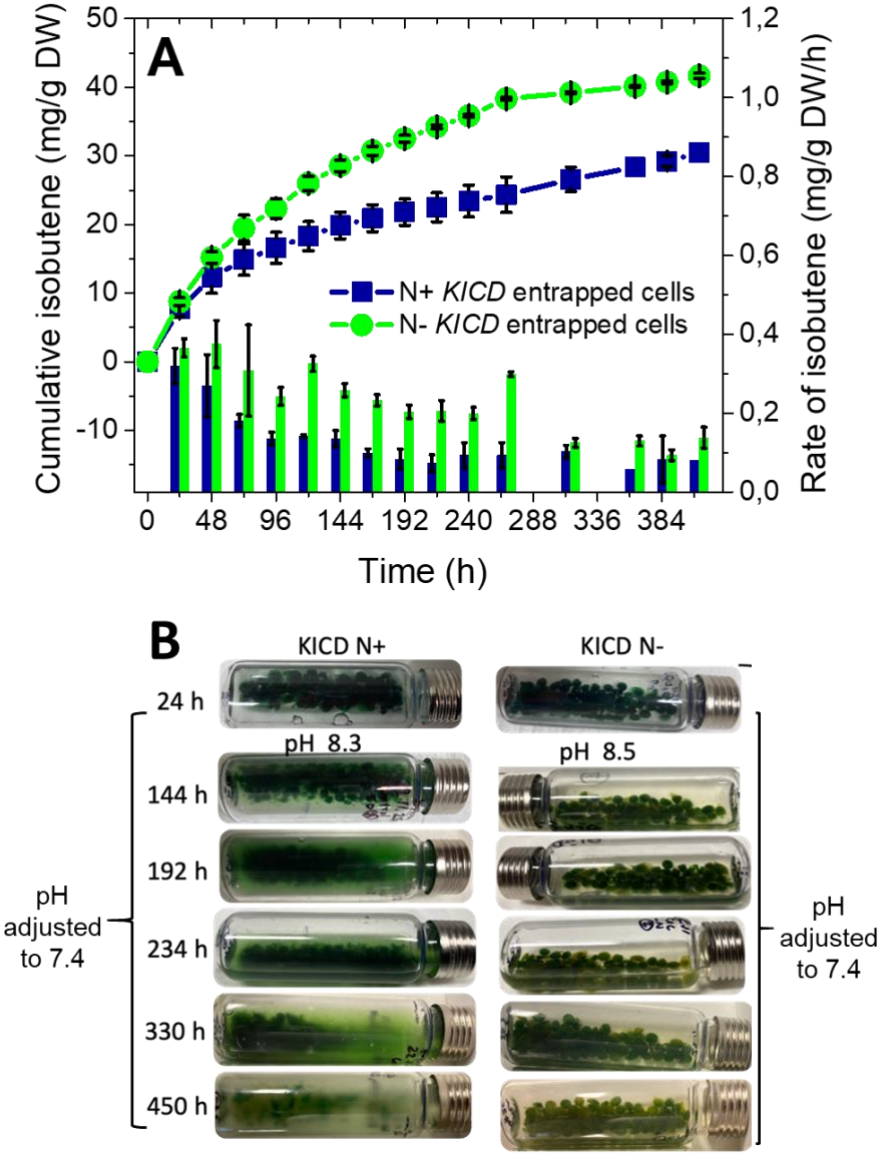

Figure 8: Implementing neutral pH and higher hydrogel amounts for entrapment of Syn-*Rn*KICD cells. A) The cumulative productivity and rate of isobutene production were monitored in the entrapped cells. B) The physical characteristics of the hydrogel beads were observed throughout the experiment. The hydrogel beads were prepared with a 5:12:1 cell: PVA: SA using H_3BO_3 and $CaCl_2$. The pH of the cultures was monitored every 24 h and adjusted to neutral (~7.4). Cells under both N+ and N- conditions were subjected to entrapment, incubated under µmol photons m^{-2} s^{-1}, and supplemented with 50 mM $NaHCO_3$ at

the start of each experiment, and 25 mM $NaHCO_3$ was added again at 216 h. The productivity of isobutene was normalized on the initial dry weight of the cells. The productivity was represented in lines, and the rates were represented in bars. These results are the average of 3 independent measurements from 3 replicates (±SD).

The N- entrapped cells showed stable bead structures and higher isobutene productivity, reaching ~41 mg/g DW at 412 h (Fig. 8), compared to N+ cells (~30 mg/g DW). No bead disintegration was observed in N- cells at this point (Fig. 8B), suggesting that the combination of N limitation and entrapment-mediated growth limitation improved isobutene production. These results suggest that under N- conditions, the entrapped cells not only prolonged their isobutene production but also delayed chlorosis, which was only slightly noticeable at 450 h (Fig. 8B), whereas free cell suspensions exhibited N-starvation-induced chlorosis within 24 h (Fig. 2B). These observations indicate that entrapping cells in PVA-SA hydrogel beads could enhance cell viability and isobutene production for an extended period under N- conditions. On the other hand, partial bead disintegration was clearly visible under N+ conditions starting at 192 h, with gradual leakage of cells into the medium, as evidenced in Fig. 8B. Despite this disintegration, isobutene production from the entrapped N+ cells continued for up to 412 h (Fig. 8A), significantly longer than in suspension cells, which only produced isobutene up to 120 h (Fig. 2A). However, the disintegrating beads eventually led to cell bleaching by 450 h (Fig. 8B). This disintegration could be due to excessive cell growth, as N+ cells tend to exhibit strong growth responses in the presence of HCO_3^- supplementation, as seen in the free cell suspension (Fig. 2A). However, entrapped cells showed delayed bleaching. These results indicate that while the twofold increase in hydrogel-to-cell ratio and maintaining neutral pH prolonged bead stability, the N+ cells still experienced delayed bleaching due to bead disintegration. Therefore, further optimization of cell entrapment methods is needed, particularly for cells under N supplementation.

Impact of a six-fold increase in the hydrogel-to-cell ratio on the stability of entrapped cell beads By employing a combination of N starved conditions and cell entrapment, we observed prolonged cell viability and enhanced isobutene production (Fig. 8). However, our attempts to restrict cell growth and increase isobutene production under N+ conditions were less effective, as seen in bead disintegration, cell leakage, gradual bleaching, and relatively lower isobutene production (Fig. 8). To address this issue, we further experimented with a 6x increase in the hydrogel to cell ratio, changing it from 5:12:1 to 5:36:3 (wet cell weight: PVA:

SA), aiming to impede cell growth and prevent bead disintegration. This modification in the cell-to-hydrogel ratio led to visually stable and distinct beads for Syn-*Rn*KICD and Syn-F336V cells (Fig. 9).

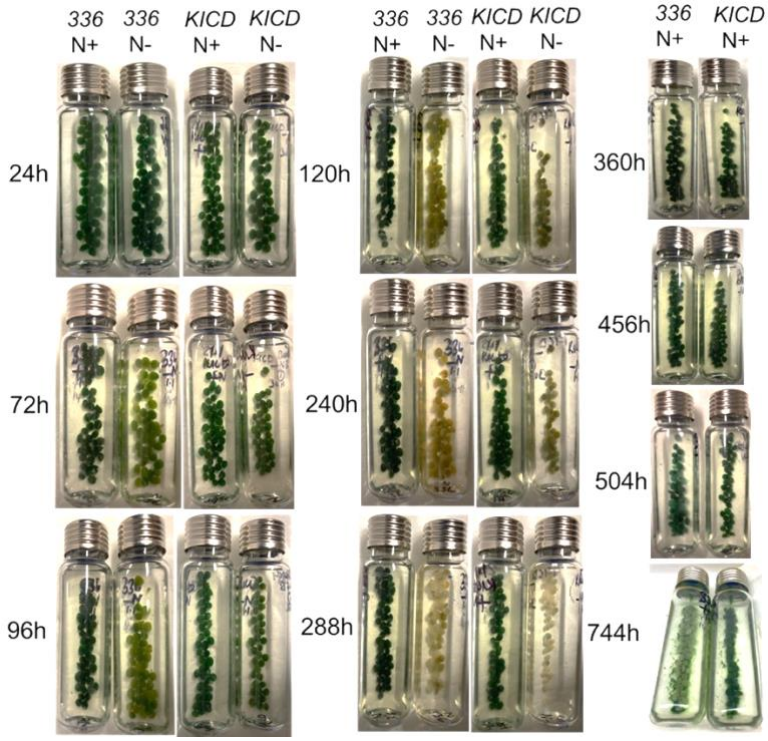

Figure 9: Entrapped Syn-F336V and Syn-*Rn*KICD cells in hydrogel beads (PVA-SA) under N+ and N- conditions. The hydrogel beads were prepared with the following ratio between the cells: PVA: SA was 5:36:3 and crosslinked with H_3BO_3 and $CaCl_2$. pH was adjusted to neutral throughout the experiments. In the picture, *336* refers to Syn-F336V and *KICD* to Syn-*Rn*KICD. The cells were illuminated under 50 µmol photons m^{-2} s^{-1} and with 50 mM $NaHCO_3$. A similar amount of initial biomass was used across all cultures.

Up to 196 h, there was no significant difference in isobutene production between N+ and N- Syn F336V cells (Fig. 10A). Interestingly, at 216 h, a notable increase in isobutene production (~67 mg/g DW) was observed in N+ Syn-F336V cells. Conversely, no further increase was observed in N- cells, which reached a maximum productivity of ~57 mg/g DW. In N+ Syn-F336V cells, isobutene production continued to rise, achieving ~91 mg/g DW at 408 h. A similar trend was observed in entrapped Syn-*Rn*KICD cells under N+ and N- conditions, with only slight differences in isobutene productivity between N+ (~38 mg/g DW) and N- (~45 mg/g DW) cells up to 216 h (Fig. 10B). After 216 h, no further increase in productivity was observed in N- cells. At this point, a significant increase in isobutene

production was observed in N+ *KICD* cells, continuing to rise until 408 h and reaching ~54 mg/g DW. The Syn-F336V and Syn-*Rn*KICD strains exhibited higher isobutene production in N+ cells than N- cells (Fig. 10A and B) after 216 h.

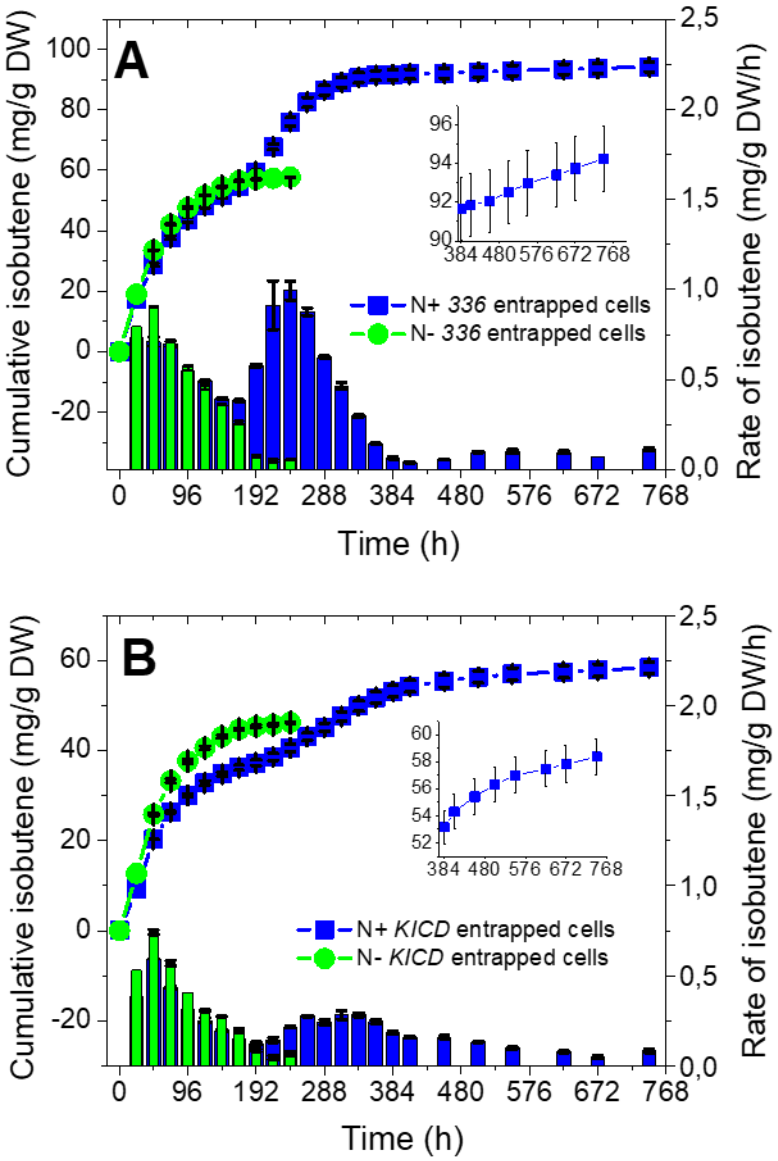

Figure 10: Entrapment of Syn-F336V and Syn-*Rn*KICD cells in the 6-time increased hydrogel amounts. The cumulative productivity (lines) and rate of isobutene (bars) in the entrapped A) Syn-F336V and B) Syn-*Rn*KICD cells under N+ and N- conditions. The beads were prepared with the following ratio between the wet cell weight and hydrogel (PVA-SA), 5:36:3, and crosslinked with H_3BO_3 and $CaCl_2$. pH was adjusted to neutral throughout the experiments. A similar amount of initial biomass was used to compare isobutene productivity across all cultures. The productivity of isobutene was normalized on the initial dry biomass of the appropriate cells. Inlets in Figures A and B showed an enlarged view of the prolonged

production of isobutene. In the figure, *336* refers to Syn-F336V, and *KICD* to Syn-*Rn*KICD. The cells were illuminated at 50 μmol photons m^{-2} s^{-1} with 50 mM $NaHCO_3$ at the start of each experiment, and 25 mM $NaHCO_3$ was added again at 408 h. These results are the average of 3 independent measurements from 3 replicates (±SD).

To further enhance isobutene production, we refreshed the cultures with BG11 medium and added 25 mM HCO_3^- at 408 h. Although the beads remained stable throughout this period, as shown by their phenotypic morphology (Fig. 9), only a slight increase in isobutene production was observed in both entrapped Syn-F336V and Syn-*Rn*KICD cells, peaking at ~94 mg/g DW and ~58 mg/g DW, respectively, at 744 h (Fig. 10). Under N+ conditions, the entrapped cell beads remained stable without disintegration (Fig. 9) and continued to produce more isobutene than N-deprived cells for up to one month (744 h) (Fig. 10). These findings suggest that the higher hydrogel-to-biomass ratio further improved bead stability, even under N+ conditions where cells tend to grow more rapidly. The results also indicate cell entrapment significantly enhances isobutene production by limiting cell growth in Syn-F336V and Syn-*Rn*KICD cells under N+ conditions.

To further demonstrate the effectiveness of entrapped cells under N+ conditions for prolonged isobutene production, we compared cell suspension and entrapped cells with similar initial biomass loading under the same production conditions. Although no significant difference in isobutene productivity was observed between free N+ cells and entrapped N+ cells up to 144 h (Fig. S6A), the suspension cells exhibited early bleaching from 144 h onward (Fig. S6B), leading to no further increase in isobutene production. In contrast, the entrapped cells showed no signs of bleaching and continued to increase isobutene production up to 744 h, achieving productivity above 1.5 times higher than their free-cell counterparts (Fig. S6A). These results further confirm that cell viability and isobutene production in entrapped Syn-F336V and Syn-*Rn*KICD cells were enhance as compared to the corresponding liquid cell cultures. When using entrapped cells to limit growth under N+ and N- conditions, we observed that N+ cells exhibited higher isobutene production than N- cells. The Syn-F336V cells showed 1.5 -fold isobutene production in N+ conditions than its corresponding N- cells, while the Syn-*Rn*KICD cells showed 1.3-fold production in N+ compared to N-. This indicates that under limited growth conditions, N availability is crucial in maintaining metabolic processes supporting isobutene production.

Therefore, we suggest that under N+ conditions, the carbon flux is effectively distributed between BCAA biosynthesis and isobutene production, allowing for the production of essential amino acids required for cellular maintenance while achieving high isobutene output in the cells. Since cell growth is restricted due to cell entrapment, N+ cells can sustain both BCAA and isobutene biosynthesis for an extended period of time, and the Syn-F336V cells showed higher isobutene production than Syn-*Rn*KICD cells (Fig.10A and B), indicating that the level of substrate available for isobutene formation is lower in the Syn-*Rn*KICD cells as compared to the Syn-F336V cells, which is in line to what has been shown (Schumann et al., 2024). In contrast, under N- conditions, both strains experience a more pronounced metabolic shift, with carbon being redirected primarily toward isobutene production at the expense of BCAA biosynthesis. The inability to produce sufficient BCAAs under nitrogen-limited conditions impairs essential cellular functions. As a result, at approximately 240 h, N- cells experience a sharp decline in isobutene production (Fig. 10), correlating with reduced cell viability (Fig. 9), probably due to a lack of essential amino acids. These results highlight three competing metabolic processes in the isobutene producing *Synechocystis* cells; one supporting cell growth and BCAA biosynthesis, one driving isobutene production and one producing homogentisate from HPP (Fig.11).

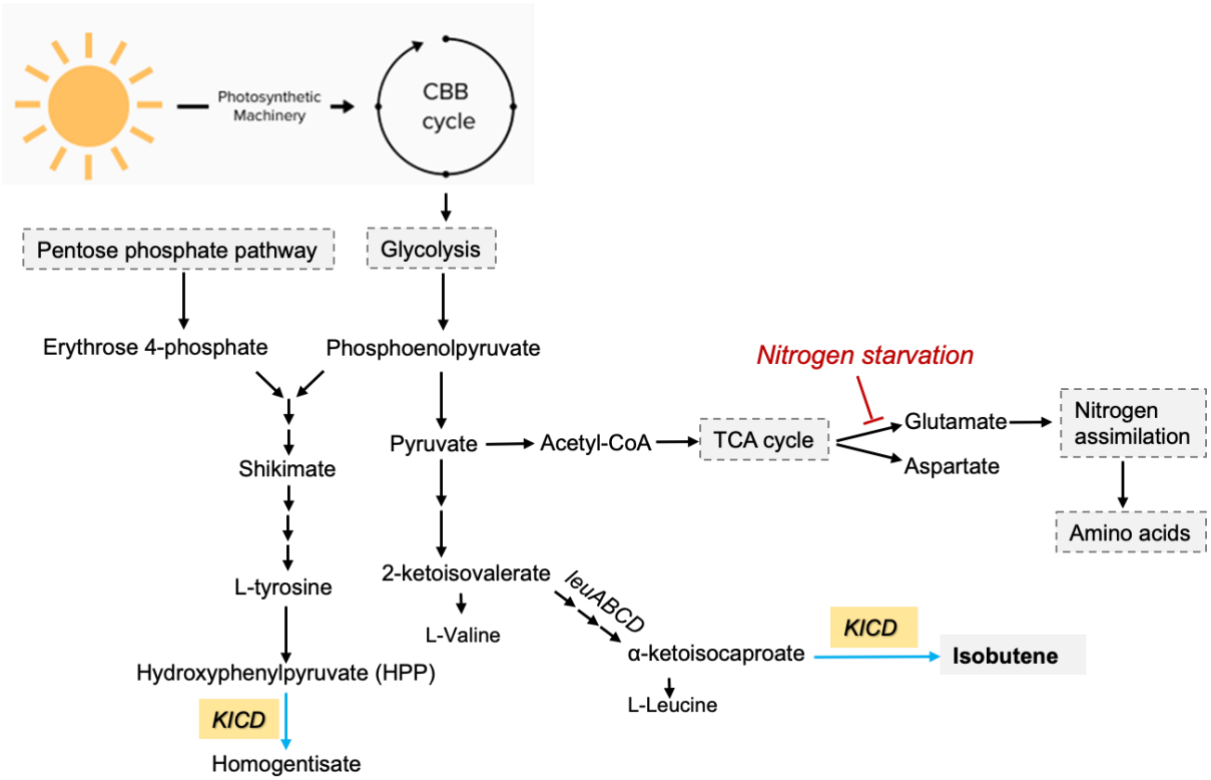

Figure 11: Schematic representation of the putative pathway for the biosynthesis of isobutene in *Synechocystis* through the introduction of α-ketoisocaproate dioxygenase (KICD) from *Rattus norvegicus* (*Rn*KICD). The black arrows indicate the native pathways, while the blue arrows represent the non-native pathways.

In the entrapped N+ cells, both the Syn-F336V and the Syn-*Rn*KICD strain maintain a balance between these processes, resulting in higher isobutene production and prolonged cell viability. However, N limitation forces the cells to prioritize isobutene synthesis, at the cost of cell viability, metabolic function and reduced productivity due to the depletion of BCAAs. This underscores the importance of nitrogen in regulating the balance between growth and isobutene production in *Synechocystis.*

Conclusion

This study demonstrated the effectiveness of using PVA-SA hydrogel for entrapping *Synechocystis* cells, leading to enhanced isobutene production over a month. The PVA-SA hydrogel beads, crosslinked with borate and calcium ions, provided stability in HCO_3^--rich environments, making them suitable for long-term use. Key factors such as crosslinking time, pH balance, and the biomass-to-hydrogel ratio were optimized to improve bead durability, restrict cell growth, prevent cell bleaching, and induce a metabolic shift toward higher isobutene production, especially when supplemented with nitrogen and carbon sources. Nitrogen availability emerged as a critical factor, with both the Syn-F336V and the Syn-*Rn*KICD strains showing significantly higher isobutene production under N+ conditions compared to N- conditions. This underscores the role of nitrogen in balancing BCAA synthesis and maximizing carbon flow toward isobutene production. Overall, the combination of PVA-SA hydrogel-based cell immobilization and precise nutrient management offers an effective strategy for improving isobutene production in *Synechocystis*, presenting a potential pathway for optimizing bio-based chemical production.

Acknowledgements

We greatly acknowledge FORMAS—A Swedish Research Council for Sustainable Development (project no. 2021-01669), The Carl Trygger Foundation for Scientific Research (CTS 23:2849), and the Swedish Energy Agency (project no. 52576-1).

Notes

The authors declare no competing financial interest.

Supporting information

The Supporting Information is available.

References

1. Abm, J. B., Oliveira, D. T. D., Mescouto, V. A. D., Dos Reis, A. S., da Rocha Filho, G. N., Santos, A. V., ... & do Nascimento, L. A. S. (2019). Optimization of light intensity and $NaNO_3$ concentration in Amazon cyanobacteria cultivation to produce biodiesel. Molecules, 24(12), 2326.
2. Aboim, J. B., Oliveira, D. T. D., Mescouto, V. A. D., Dos Reis, A. S., da Rocha Filho, G. N., Santos, A. V., ... & do Nascimento, L. A. S. (2019). Optimization of light intensity and $NaNO_3$ concentration in Amazon cyanobacteria cultivation to produce biodiesel. Molecules, 24(12), 2326.
3. Allen, M. M., Law, A., & Evans, E. H. (1990). Control of photosynthesis during nitrogen depletion and recovery in a non-nitrogen-fixing cyanobacterium. Archives of Microbiology, 153, 428-431.
4. Allen, M. M., & Smith, A. J. (1969). Nitrogen chlorosis in blue-green algae. Archiv für Mikrobiologie, 69(2), 114–120.
5. Angermayr, S. A., Rovira, A. G., & Hellingwerf, K. J. (2015). Metabolic engineering of cyanobacteria for the synthesis of commodity products. Trends in Biotechnology, 33(6), 352-361.
6. Badger, M. R., & Price, G. D. (2003). CO_2 concentrating mechanisms in cyanobacteria: molecular components, their diversity and evolution. Journal of Experimental Botany, 54(383), 609-622.
7. Bolto, B., Tran, T., Hoang, M., & Xie, Z. (2009). Crosslinked poly (vinyl alcohol) membranes. Progress in Polymer Science, 34(9), 969-981.
8. Brouers, M., & Hall, D. O. (1986). Ammonia and hydrogen production by immobilized cyanobacteria. Journal of Biotechnology, 3(5-6), 307-321.
9. Carroll, A. L., Case, A. E., Zhang, A., & Atsumi, S. (2018). Metabolic engineering tools in model cyanobacteria. Metabolic Engineering, 50, 47-56.
10. Cheng, A. T. Y., & Rodriguez, F. (1981). Mechanical properties of borate crosslinked poly (vinyl alcohol) gels. Journal of Applied Polymer Science, 26(11), 3895-3908.
11. Chisti, Y. (2007). Biodiesel from microalgae. Biotechnology Advances, 25(3), 294-306.
12. Choe, S., You, S., Park, K., Kim, Y., Park, J., Cho, Y., ... & Myung, J. (2024). Boric acid-crosslinked poly (vinyl alcohol): biodegradable, biocompatible, robust, and high-barrier paper coating. Green Chemistry.
13. Ducat, D. C., Way, J. C., & Silver, P. A. (2011). Engineering cyanobacteria to generate high-value products. Trends in Biotechnology, 29(2), 95-103.
14. Farrokh, P., Sheikhpour, M., Kasaeian, A., Asadi, H., & Bavandi, R. (2019). Cyanobacteria as an eco-friendly resource for biofuel production: a critical review. Biotechnology Progress, 35(5), e2835.
15. Forchhammer, K., & Schwarz, R. (2019). Nitrogen chlorosis in unicellular cyanobacteria–a developmental program for surviving nitrogen deprivation. Environmental Microbiology, 21(4), 1173-1184.
16. Forchhammer, K., & Selim, K. A. (2020). Carbon/nitrogen homeostasis control in cyanobacteria. FEMS Microbiology Reviews, 44(1), 33-53.
17. Gohil, J. M., Bhattacharya, A., & Ray, P. (2006). Studies on the crosslinking of poly (vinyl alcohol). Journal of Polymer Research, 13, 161-169.
18. Gordillo, F. J., Goutx, M., Figueroa, F. L., & Niell, F. X. (1998). Effects of light intensity, CO_2 and nitrogen supply on lipid class composition of Dunaliella viridis. Journal of Applied Phycology, 10, 135-144.
19. Hauge, K., Bergene, E., Chen, D., Fredriksen, G. R., & Holmen, A. (2005). Oligomerization of isobutene over solid acid catalysts. Catalysis Today, 100(3-4), 463-466.
20. Hua, S., Ma, H., Li, X., Yang, H., & Wang, A. (2010). pH-sensitive sodium alginate/poly (vinyl alcohol) hydrogel beads prepared by combined Ca^{2+} crosslinking and freeze-thawing cycles for controlled release of diclofenac sodium. International Journal of Biological Macromolecules, 46(5), 517-523.

21. Hulnik, M., Trofimuk, D., Nikishau, P. A., Kiliclar, H. C., Kiskan, B., & Kostjuk, S. V. (2023). Visible-light-induced cationic polymerization of isobutylene: a route toward the synthesis of end-functional polyisobutylene. ACS Macro Letters, 12(8), 1125-1131.
22. Kim, H. W., Vannela, R., Zhou, C., & Rittmann, B. E. (2011). Nutrient acquisition and limitation for the photoautotrophic growth of Synechocystis sp. PCC6803 as a renewable biomass source. Biotechnology and Bioengineering, 108(2), 277-285.
23. Kosourov, S. N., He, M., Allahverdiyeva, Y., & Seibert, M. (2018). Immobilization of microalgae as a tool for efficient light utilization in H_2 production and other biotechnology applications.
24. Kosourov, S., Leino, H., Murukesan, G., Lynch, F., Sivonen, K., Tsygankov, A. A., ... & Allahverdiyeva, Y. (2014). Hydrogen photoproduction by immobilized N_2-fixing cyanobacteria: understanding the role of the uptake hydrogenase in the long-term process. Applied and Environmental Microbiology, 80(18), 5807-5817.
25. Kostjuk, S. V. (2015). Recent progress in the Lewis acid co-initiated cationic polymerization of isobutylene and 1,3-dienes. RSC Advances, 5(17), 13125-13144.
26. Lichtenthaler, H. K. (1987). [34] Chlorophylls and carotenoids: pigments of photosynthetic biomembranes. In Methods in Enzymology (Vol. 148, pp. 350-382). Academic Press.
27. Lindberg, P., Park, S., & Melis, A. (2010). Engineering a platform for photosynthetic isoprene production in cyanobacteria, using Synechocystis as the model organism. Metabolic Engineering, 12(1), 70-79.
28. Markou, G., Vandamme, D., & Muylaert, K. (2014). Microalgal and cyanobacterial cultivation: the supply of nutrients. Water Research, 65, 186-202.
29. Melis, A. (2009). Solar energy conversion efficiencies in photosynthesis: minimizing the chlorophyll antennae to maximize efficiency. Plant Science, 177(4), 272-280.
30. Miller, A. G., & Colman, B. (1980). Evidence for HCO_3^- transport by the blue-green alga (cyanobacterium) Coccochloris peniocystis. Plant Physiology, 65(2), 397-402.
31. Miller, A. G., Espie, G. S., & Canvin, D. T. (1990). Physiological aspects of CO_2 and HCO_3^- transport by cyanobacteria: a review. Canadian Journal of Botany, 68(6), 1291-1302.
32. Mustila, H., Kugler, A., & Stensjö, K. (2021). Isobutene production in Synechocystis sp. PCC 6803 by introducing α-ketoisocaproate dioxygenase from Rattus norvegicus. Metabolic Engineering Communications, 12, e00163.
33. Nicholas, C. P. (2017). Applications of light olefin oligomerization to the production of fuels and chemicals. Applied Catalysis A: General, 543, 82-97.
34. Pedruzi, G. O., Amorim, M. L., Santos, R. R., Martins, M. A., & Vaz, M. G. (2019). Biomass accumulation-influencing factors in microalgae farms. Revista Brasileira de Engenharia Agrícola e Ambiental, 24, 134-139.
35. Peters, M. W., & Taylor, J. D. (2013). U.S. Patent No. 8,373,012. Washington, DC: U.S. Patent and Trademark Office.
36. Rana, A., Gomes, L. C., Rodrigues, J. S., Yacout, D. M., Arrou-Vignod, H., Sjölander, J., ... & Ottosson, H. (2022). A combined photobiological–photochemical route to C 10 cycloalkane jet fuels from carbon dioxide via isoprene. Green Chemistry, 24(24), 9602-9619.
37. Rebolledo-Leiva, R., Moreira, M. T., & González-García, S. (2022). Offsetting the environmental impacts of single or multi-product biorefineries from wheat straw. Bioresource Technology, 361, 127698.
38. Rissanen, V., Vajravel, S., Kosourov, S., Arola, S., Kontturi, E., Allahverdiyeva, Y., & Tammelin, T. (2021). Nanocellulose-based mechanically stable immobilization matrix for enhanced ethylene production: a framework for photosynthetic solid-state cell factories. Green Chemistry, 23(10), 3715-3724.
39. Rodrigues, J. S., Kovács, L., Lukeš, M., Höper, R., Steuer, R., Červený, J., ... & Zavřel, T. (2023). Characterizing isoprene production in cyanobacteria–insights into the effects of light, temperature, and isoprene on Synechocystis sp. PCC 6803. Bioresource Technology, 380, 129068.
40. Rossoni, L., Hall, S. J., Eastham, G., Licence, P., & Stephens, G. (2015). The putative mevalonate diphosphate decarboxylase from Picrophilus torridus is in reality a mevalonate-3-kinase with high potential for bioproduction of isobutene. Applied and Environmental Microbiology, 81(7), 2625-2634.

41. Sabourin, P. J., & Bieber, L. L. (1982). Purification and characterization of an alpha-ketoisocaproate oxygenase of rat liver. *Journal of Biological Chemistry*, *257*(13), 7460-7467.
42. Santos-Merino, M., Singh, A. K., & Ducat, D. C. (2019). New applications of synthetic biology tools for cyanobacterial metabolic engineering. Frontiers in Bioengineering and Biotechnology, 7, 33.
43. Sauer, J., Schreiber, U., Schmid, R., Völker, U., & Forchhammer, K. (2001). Nitrogen starvation-induced chlorosis in *Synechococcus* PCC 7942. Low-level photosynthesis as a mechanism of long-term survival. Plant Physiology, 126(1), 233-243.
44. Simpson, N. E., Stabler, C. L., Simpson, C. P., Sambanis, A., & Constantinidis, I. (2004). The role of the $CaCl_2$–guluronic acid interaction on alginate encapsulated βTC3 cells. Biomaterials, 25(13), 2603-2610.
45. Spat, P., Klotz, A., Rexroth, S., Macek, B., & Forchhammer, K. (2018). Chlorosis as a developmental program in cyanobacteria: the proteomic fundament for survival and awakening. Molecular & Cellular Proteomics.
46. Schumann, C., Kugler, A., Berggren G., Land, H., Blikstad, C., & Stensjö, K. (2024). Structure-guided engineering of α-ketoisocaproate dioxygenase increases isobutene production in *Synechocystis* sp. PCC 6803. bioRxiv 2024.12.20.629387; doi: https://doi.org/10.1101/2024.12.20.629387.
47. Taylor, J. D., Jenni, M. M., & Peters, M. W. (2010). Dehydration of fermented isobutanol for the production of renewable chemicals and fuels. Topics in Catalysis, 53, 1224-1230.
48. Tóth, G. S., Siitonen, V., Nikkanen, L., Sovic, L., Kallio, P., Kourist, R., ... & Allahverdiyeva, Y. (2022). Photosynthetically produced sucrose by immobilized Synechocystis sp. PCC 6803 drives biotransformation in E. coli. Biotechnology for Biofuels and Bioproducts, 15(1), 146.
49. Van Alphen, P., Abedini Najafabadi, H., Branco dos Santos, F., & Hellingwerf, K. J. (2018). Increasing the photoautotrophic growth rate of Synechocystis sp. PCC 6803 by identifying the limitations of its cultivation. Biotechnology Journal, 13(8), 1700764.
50. van Leeuwen, B. N., van der Wulp, A. M., Duijnstee, I., van Maris, A. J., & Straathof, A. J. (2012). Fermentative production of isobutene. Applied Microbiology and Biotechnology, 93, 1377-1387.
51. Vajravel, S., Sirin, S., Kosourov, S., & Allahverdiyeva, Y. (2020). Towards sustainable ethylene production with cyanobacterial artificial biofilms. Green Chemistry, 22(19), 6404-6414.
52. Valsami, E. A., Pateraki, A., Melis, A., & Ghanotakis, D. F. (2021). Heterologous β-phellandrene production by alginate immobilized Synechocystis sp. PCC 6803. Journal of Applied Phycology, 33, 2157-2168.
53. Wilson, J., Gering, S., Pinard, J., Lucas, R., & Briggs, B. R. (2018). Bio-production of gaseous alkenes: ethylene, isoprene, isobutene. Biotechnology for Biofuels, 11, 1-11.
54. Wu, J., Liu, R., Zhang, W., Zhong, Q., Lei, Y., & Huang, L. (2024). Enhancement of mechanical behaviors of the 3D-printed polyvinyl alcohol–based scaffold by boric acid crosslinking. Journal of Polymer Engineering, 44(4), 251-262.
55. Wu, K. Y. A., & Wisecarver, K. D. (1992). Cell immobilization using PVA crosslinked with boric acid. Biotechnology and Bioengineering, 39(4), 447-449.
56. Zhong, Y., Lin, Q., Yu, H., Shao, L., Cui, X., Pang, Q., ... & Hou, R. (2024). Construction methods and biomedical applications of PVA-based hydrogels. Frontiers in Chemistry, 12, 1376799.
57. Zhu, X. G., Long, S. P., & Ort, D. R. (2008). What is the maximum efficiency with which photosynthesis can convert solar energy into biomass? Current Opinion in Biotechnology, 19(2), 153-159.